Kinetics of phase separation and coarsening in dilute surfactant pentaethylene glycol monododecyl ether solutions

S. Tanaka,[a] Y. Kubo, Y. Yokoyama, A. Toda, K. Taguchi, and H. Kajioka
Graduate School of Integrated Arts and Sciences, Hiroshima University, 1-7-1 Kagamiyama, Higashi-Hiroshima 739-8521, Japan

(Received 4 August 2011; accepted 22 November 2011; published online 15 December 2011)

We investigated the phase separation phenomena in dilute surfactant pentaethylene glycol monododecyl ether ($C_{12}E_5$) solutions focusing on the growth law of separated domains. The solutions confined between two glass plates were found to exhibit the phase inversion, characteristic of the viscoelastic phase separation; the majority phase (water-rich phase) nucleated as droplets and the minority phase (micelle-rich phase) formed a network temporarily, then they collapsed into an usual sea-island pattern where minority phase formed islands. We found from the real-space microscopic imaging that the dynamic scaling hypothesis did not hold throughout the coarsening process. The power law growth of the domains with the exponent close to 1/3 was observed even though the coarsening was induced mainly by hydrodynamic flow, which was explained by Darcy's law of laminar flow. [doi:10.1063/1.3668349]

I. INTRODUCTION

The dynamics of liquid-liquid phase separation has been intensively studied so far both theoretically and experimentally. The dynamic scaling hypothesis, assuming that the structure of a phase separating system is characterized by a single length scale, l, has played a central role in developing theories[1–5] and has brought great success in interpreting experimental observations. Especially, the growth of the length scale obeys a power law, $l \sim t^{\alpha}$, which has been derived theoretically under the dynamic scaling hypothesis and has been confirmed by many experiments.[6–17]

Recently, however, it was found that fluid systems where their viscoelastic behavior affects the process of phase separation do not exhibit the dynamic scaling. This class of phase separation is called the viscoelastic phase separation[18] and is found in a variety of materials such as polymer solutions,[19–21] polymer mixtures,[22] colloidal suspensions,[23] and protein solutions.[24]

Interestingly, the power law growth of the length scale in the viscoelastic phase separation has been observed in experiments[19–24] and in simulations[25–31] even though the dynamic scaling did not hold there. Taniguchi and Onuki,[25] for example, showed with a simulation for polymer solutions that the growth exponent α became 1/3 when their fluid had viscoelasticity, whereas $\alpha = 2/3$ when it did not. The high value of α is believed to be a result of the hydrodynamic ($\alpha = 1$) or the inertial hydrodynamic ($\alpha = 2/3$) coarsening mode. In their simulations, the viscoelasticity suppressed hydrodynamic flows and allowed only diffusive domain growth. It is known that coexistence of different coarsening modes by itself breaks down the dynamic scaling.[32] There are other simulation studies reported the value of α close to 1/3 (Refs. 26, 28, and 30) or other values.[29]

Experimentally, the growth law of the viscoelastic phase separation was studied mainly for polymer solutions,[19–21] where $\alpha = 0.1 - 0.3$ was reported. Tanaka and co-workers also reported $\alpha = 0.5$ for colloidal suspensions[23] and for protein solutions.[24]

So far as above, the growth law in the viscoelastic phase separation has not yet been established well. It may be strongly dependent on material properties.[28] Its slow coarsening (lower α than those in the hydrodynamic mode) has been attributed to suppression of hydrodynamic flows due to the viscoelasticity.[25] However, it is shown experimentally in this report that the hydrodynamic flows may be a main coarsening mechanism even in the viscoelastic phase separation processes.

We use dilute surfactant pentaethylene glycol monodedecyl ether ($C_{12}E_5$) solutions as a model system to investigate the coarsening mechanism of the viscoelastic phase separation. We show that the system exhibits behaviors characteristic of the viscoelastic phase separation even when the concentration of the surfactant is as low as 2 wt. %. While it was reported that the system exhibited peculiar phase separation patterns,[33] it is the first time that the phase separation of the system was treated as a viscoelastic phase separation, and that the coarsening process was investigated in detail.

We found that flows played a dominant role in the coarsening process of our system, and that at the same time experimentally determined growth exponents were close to 1/3, which was lower than the values known for the hydrodynamic coarsening mode. This is explained by Darcy's law of laminar flow, which suggests that the viscoelasticity relaxes completely in the stage of coarsening. In this context, we discuss the role of viscoelasticity in phase separation dynamics and pattern evolution.

This paper is organized as follows. In Sec. II, we describe the details of our experimental procedures and methods for analyzing phase separation patterns obtained. In Sec. III, the results of our experiments are shown. Section IV is devoted

[a]Electronic mail: shinpei@hiroshima-u.ac.jp.

to the discussion how to interpret our results, where a simple model to produce experimentally observed growth exponent is presented. Finally in Sec. V, we summarize the paper.

II. EXPERIMENTS

Non-ionic surfactant, pentaethylene glycol monododecyl ether ($C_{12}E_5$) was purchased from Wako Chemicals, Osaka. An appropriate amount of surfactant was dissolved in deionized and filtered water as a mother solution. We use the wt. % for the concentration of the surfactant, c. A fluorescent dye eosin Y (Sigma-Aldrich, Tokyo) was used to label $C_{12}E_5$ micelles. An appropriate amount of aqueous eosin Y mother solution (0.05 wt. %) was added to $C_{12}E_5$ solutions to make the final weight ratio of eosin Y to the surfactant 5×10^{-4}. It was found that the dye was preferentially distributed into the micelles as shown later. The labeled samples were sandwiched between two glass cover slips of 24 mm and 15 mm in diameter. The thickness, d, of the samples was set at about 20 μm with aluminum foil spacers. The glass rims were sealed with glue to prevent evaporation.

The sample cell was stuck with paraffin oil on a copper plate of 2 mm thickness whose temperature was measured by a thermocouple. The temperature was controlled within $\pm 0.2\,^{\circ}$C by an aluminum block with a heater. The block was exchangeable and two blocks kept at different temperatures were used for a temperature jump.

The sample temperature was first kept just below the coexistence temperature for 10 min and then was raised to a designated phase separation temperature. The solutions exhibited a lower critical-solution-temperature-type phase diagram as shown in Fig. 1. The rate of the temperature change was typically 3–6 °C/min. These slow rates mean that the phase separation proceeded during the temperature jump. Fluorescence images were taken using a confocal laser microscope (Eclipse TE2000-E, Nikon, Tokyo) with a 20 mW solid-state laser of a wavelength of 488 nm. With a low magnitude objective lens, Nikon Plan Fluor 4×, numerical aperture 0.13, and a wide confocal aperture of 150 μm, samples were illuminated roughly uniformly in z-direction. We confirmed that the laser beam did not cause any significant temperature change at the spot even if we set the scan rate very low. The phase field microscopy was also used to observe a fine structure of domains.

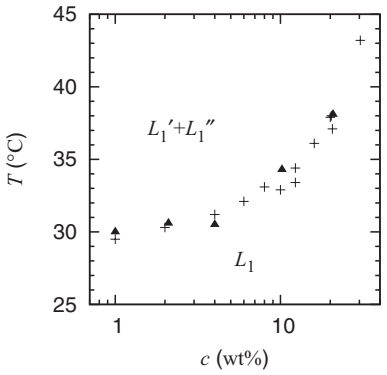

FIG. 1. A phase diagram of dilute $C_{12}E_5$ solutions. Crosses and filled triangles represent cloud points with and without eosin Y, respectively.

The images obtained were analyzed digitally to extract information of domain coarsening. The area fraction A, interface density L, the Euler characteristic χ were calculated by a black-and-white operation on the images. A is defined as the ratio of the micelle-rich domain area to the total area. L is the number of pixels at the interface between separated domains divided by the total number of pixels. Thus L is also dimensionless. The growth exponent, α, was extracted by fitting L with the function $L \sim t^{-\alpha}$, where t is the elapsed time measured from the onset of the separation. Obtained values of α were averaged over at least four independent experiments.

The Euler characteristic, χ, was calculated according to the method reported in the literature.[35,36] χ is a topological measure describing the interface connectivity. In two dimension, χ is equal to integral of the curvature along interfaces, thus χ/L gives the mean curvature of domains.

The cloud points of the mixtures were determined either by the light scattering or by the transmission with an Ar-ion laser (Melles Griot, Tokyo) of a wavelength of 488 nm. A 100 μl sample solution was put into a cylindrical glass cell, which was then immersed in a heat bath of decalin. The temperature of the heat bath was controlled by circulating water. At the transition, the solution became cloudy and the scattering intensity increased or the transmission of light decreased. The point where the change started was defined as the cloud point.

III. RESULTS

A. Phase diagram

Figure 1 shows a phase diagram of dilute $C_{12}E_5$ solutions with and without eosin Y. It plots the cloud points where the separation between L_1' (dilute micellar phase) and L_1'' (dense micellar phase) occurred, which are relevant to this study. We call L_1' the water-rich phase and L_1'' the micelle-rich phase. The cloud points of the solutions containing eosin Y were identical within an experimental error with those without eosin Y, which suggests that eosin Y does not affect the phase separation. Obtained phase diagram was also consistent with the literature.[34]

B. Network pattern formation

Figure 2 shows a process of phase separation observed in a 2.0 wt. % $C_{12}E_5$ solution at 4.4 °C above the cloud point. After the temperature jump, water-rich domains (darker regions) first nucleated in the mother phase [Fig. 2(a)] even if the water-rich phase was the majority phase. The concentration of $C_{12}E_5$ outside the water-rich domains was not homogeneous, but there were characteristic "rims" around the water-rich domains; the concentration of the rims was higher (the fluorescence was brighter) than that of the mother phase [Figs. 2(a) and 6].

Then the water-rich domains grew to collide and coalesce with their neighbors, which resulted in a network pattern of the micelle-rich domains [Fig. 2(b)]. The coarsening of the micelle-rich networks proceeded as occasional breaks of the elongated domains ("branches") and shrinks of them

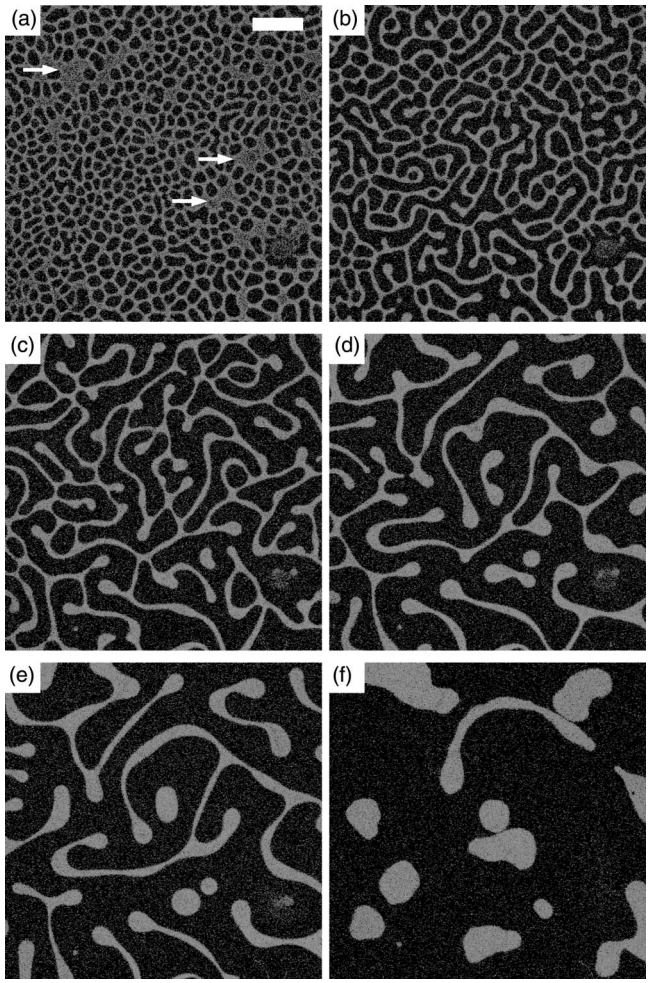

FIG. 2. The phase separation process of 2.0 wt. % $C_{12}E_5$. The brighter the region, the higher the micelle concentration. The temperature was raised from 30.5 °C to 34.9 °C. The time of the observation from the onset of the separation was: 12 s (a); 32 s (b); 72 s (c); 172 s (d); 372 s (e); 1172 s (f). Arrows in (a) indicate a region where the mother phase still remains. The scale bar is 0.5 mm.

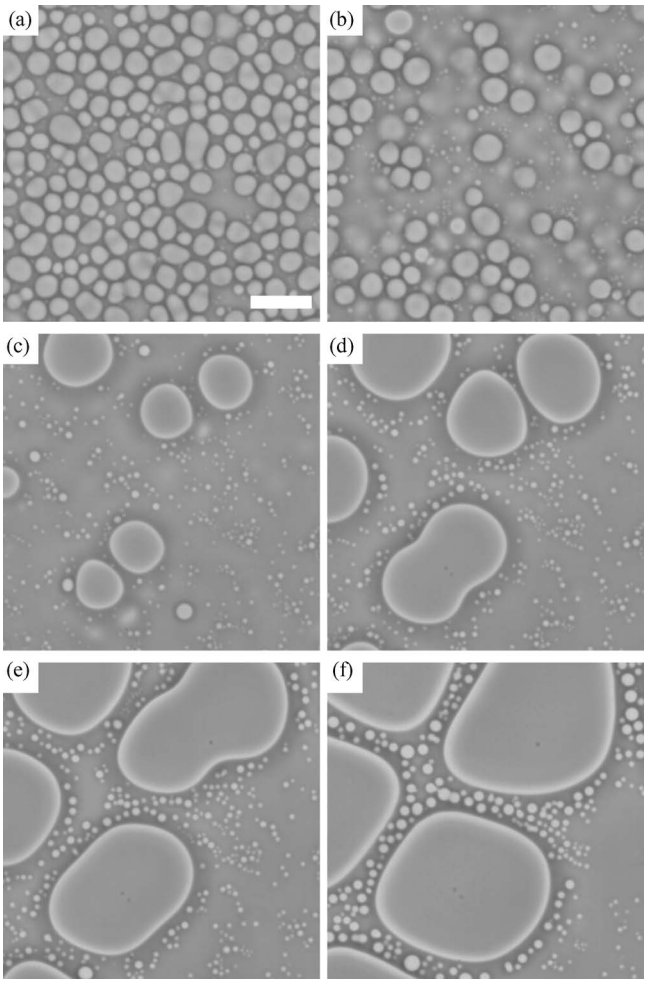

FIG. 3. The nucleation process of 2.0 wt. % $C_{12}E_5$ in the very early stage of the phase separation. The temperature was raised from 30.0 °C to 35.0 °C. The time of observation from the onset of the separation was: 4 s (a); 5 s (b); 6 s (c); 7 s (d); 8 s (e); 11 s (f). The scale bar is 0.05 mm.

[Figs. 2(b)–2(e)]. The coexistence between circular domains and elongated branches was evident in the late stage of the coarsening [Figs. 2(d)–2(f)], which suggests the breakdown of the dynamic scaling hypothesis. In the final stage, the micelle-rich domains became circular, which was consistent with the fact that the micelle-rich phase was the minority phase according to the phase diagram (Fig. 1). This result also indicated that the fluorescent molecules were preferentially distributed into the micelle-rich phase.

C. Fine structure and wetting phenomena

Using the phase contrast imaging technique, we found that there were fine structures in the phase separation patterns as shown in Fig. 3, which were not detected by the fluorescence imaging. The network of micelle-rich domains contained inside a number of small droplets of the water-rich phase. The similar fine structure has been reported in the literature.[33] It should be noted that the sample contained the dye for the sake of standardization, thus the fine structure shown in Fig. 3 was not a result of its absence. The magnification of Fig. 3 is about ten times larger than that of Fig. 2. The reason why these fine structures were not observed with the confocal fluorescence microscopy was probably because we used a low numerical aperture objective lens and a wide confocal aperture to illuminate samples uniformly in z-direction, and thus small bubbles in the domains were averaged out. We sometimes actually observed bubbles in fluorescence images if they were large enough to be detected.

The phase separation began with the nucleation of many water-rich domains [Fig. 3(a)], whose size was about an order of magnitude smaller than those observed with the fluorescence microscopy [Fig. 2(a)]. It seemed that the water-rich domains did not yet form a bridge between the two glass plates in this stage, judging from slight shadows of background domain structure seen in water-rich domains. Majority of the water-rich domains, however, did not grow further but disappeared one by one [Fig. 3(b)]. The mechanism of this disappearance or where they have gone is unclear, though the wetting phenomena likely play a significant role here. Note that glass surfaces are more wettable by water-rich domains than by micelle-rich domains.

Some of the water-rich domains remained and began to grow [Figs. 3(c)–3(e)]. The domains larger than about 50 μm with sharp edges formed a bridge between two glass plates since the gap d was 20 μm and little fluorescence was observed in these domains. We could not observe whether the bridges were formed from domains attached on the glass surface or from domains inside the solution. In this stage, a number of tiny water-rich droplets also survived, or possibly created by the interface-quench effect,[37] making the size distribution of the water-rich domains bimodal. While the larger water-rich domains grew, the micelle-rich domains formed a network containing tiny "bubbles" of the water-rich phase [Fig. 3(f)]. It was from this stage where the fluorescence observation could detect the pattern formation.

The water-rich bubbles in the micelle-rich domains occasionally coalesced with each other and gradually disappeared in such a way that they were absorbed into wetting layers on the glass plates. Therefore, this fine structure eventually disappeared completely, but it usually took a few hundred seconds. We did not use these images of the fine structure for the further analysis in this study, since it was not straightforward how to extract information of domains from these images. Therefore, the analyses shown hereafter were done only on the fluorescence images ignoring the fine structure. The existence of small bubbles, however, was utilized later for the detection of flow [Fig. 7].

It is known that wetting on solid walls by a separated phase induces a long-range attraction between domains of that phase.[38] The attraction operates only when the two domains are connected through the wetting layers. Between water-rich domains observed in our solutions, however, this attraction did not work judging from the flattened boundaries between two adjacent domains [Figs. 3(c)–3(f)]; they were actually repelled by each other and it took a while for them to merge after collision. This suggests that either the wetting layers of the water-rich phase were not connected with each other (partial wetting), or the micelle-rich domain in between two water-rich domains became too hard to be deformed easily.

D. Morphology characteristics

Figure 4 shows three morphology characteristics and their combination obtained for the pattern shown in Fig. 2. After the quick increase of the area fraction A and the interface density L, they began to decrease. The coarsening process was considered to start at the time when the decrease began ($t \simeq 10$ s). The slow shrinking of the domains during the coarsening process was reported as an important mark of the viscoelastic phase separation.[18] Figure 4(b) shows that L decreased according to the power law with an exponent close to 1/3.

The mean curvature of interfaces is given by (total number of pixels) $\times$ (χ/L). Since L is always positive, χ shown in Fig. 4(c) indicates that the mean curvature of domains seen from micelle-rich domains changed from negative to positive. This is a clear evidence of the phase inversion, where the water-rich phase (the majority phase) nucleates as discs at first, whereas the micelle-rich phase

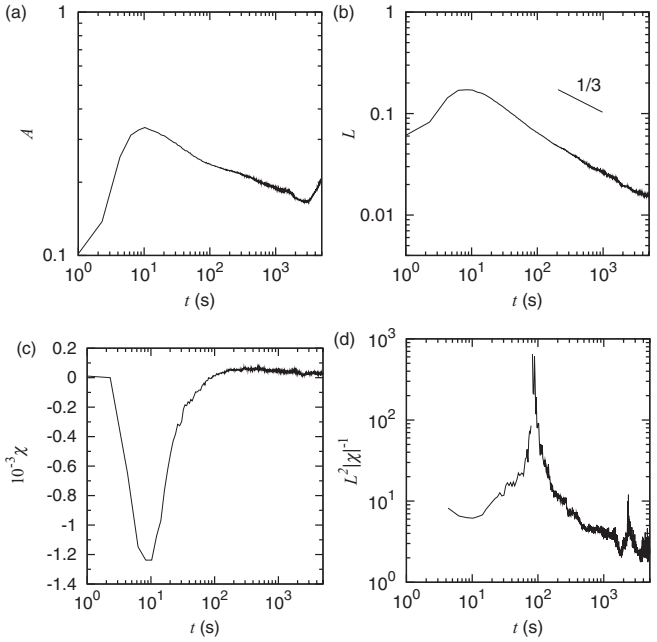

FIG. 4. The morphology characteristics calculated for the pattern shown in Fig. 2: the area fraction A (a); the interface density L (b); the Euler characteristic χ (c). The scaling hypothesis is tested by plotting $L^2/|\chi|$ in (d).

(the minority phase) forms discs at last. This phase inversion started at the beginning of the coarsening process, $t \simeq 100$ s in this sample. The quick decrease of $|\chi|$ before the inversion indicated elongation of micelle-rich domains.

If a pattern evolution can be described in terms of the dynamic scaling hypothesis, the relation

$$L \sim l^{-1}, \quad |\chi| \sim l^{-2} \tag{1}$$

should be realized,[35] where l is the characteristic length of the pattern. This means that $L^2/|\chi|$ becomes a constant. Figure 4(d) shows the change of $L^2/|\chi|$ with time. It is clear that $L^2/|\chi|$ was not a constant at any stage of the phase separation, suggesting that the scaling hypothesis cannot be applied on the systems observed.

E. Growth exponent

Figure 5 shows the ΔT dependence of the growth exponent α. Each point was an average of 4–6 independent experiments. An example of the error shown in Fig. 5 was estimated as the standard deviation of the data. Overall, the value of α was around 1/3, and the error was less than ± 0.1. It can be seen that α tended to increase with the increase of ΔT.

IV. DISCUSSION

A. Nucleation, coarsening, and phase inversion

First of all, let us discuss the overall process of the phase separation. The phase separation starts with a complex nucleation process of water-rich domains in the mother phase [Figs. 3 and 2(a)] even though they are the majority phase. The nucleation process likely involves the wetting

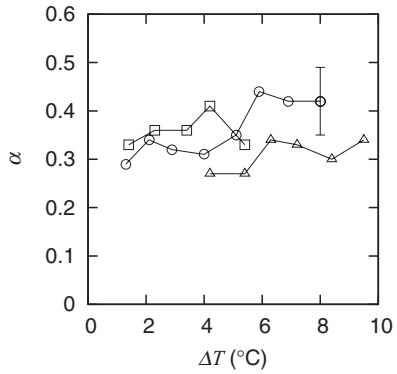

FIG. 5. The growth exponent α versus temperature jump ΔT. Symbols represent: squares 2 wt. %; circles 4 wt. %; triangles 8 wt. %. An error bar was calculated as the standard deviation of the data from six independent experiments.

phenomena on cover slips as suggested by the disappearance of small water-rich droplets shown in Figs. 3(a) and 3(b).

After the formation of well-defined water-rich nuclei, which bridges between two glass plates, characteristic "rims" of the micelle-rich phase (brighter than the mother phase) are formed around them [Fig. 2(a)]. An example of the fluorescence intensity profile from the center of a water-rich domain is shown in Fig. 6. The width of the rim is 20–30 μm and the intensity is about twice higher than that in the mother phase. Given that the fluorescent molecules are preferentially distributed into micelles, the high intensity of the rims indicates the high concentration of micelles.

The situation may have a resemblance to a hole punctured in an elastic membrane under a tension. A part of the membrane released from the tension by the hole shrinks around it. Thus the existence of the rims suggests that the mother phase behaves elastically when water-rich domains nucleate. Indeed, it is considered that this elastic nature of the mother phase induces the nucleation of the majority phase, since the elasticity resists diffusion of micelles to aggregate. The origin of this elasticity may come from entanglement of wormlike micelles of $C_{12}E_5$.[39]

This behavior has been explicitly simulated using a disconnectable spring model by Araki and Tanaka, and they found arrays of nucleated droplets in their simulation (Fig. 11 in Ref. 40), which is similar to what we observed in the nucleation stage [Fig. 2(a)], where arrays of nucleated water-rich domains are formed. However, they did not mention about the formation of rims around nuclei probably because of limited number of particles in their simulation.

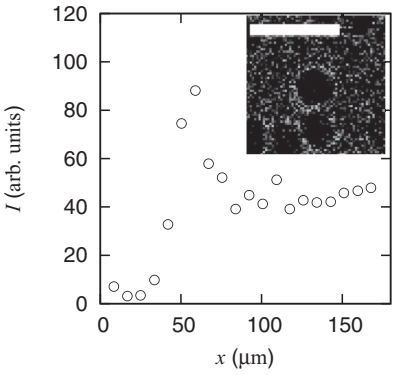

FIG. 6. Fluorescence intensity profile around a water-rich domain nucleated in the mother phase. The distance x was measured from the center of a water-rich domain. The domain used to calculate the profile, which was found in the same sample as the one shown in Fig. 2, is shown in the inset. The scale bar is 0.25 mm.

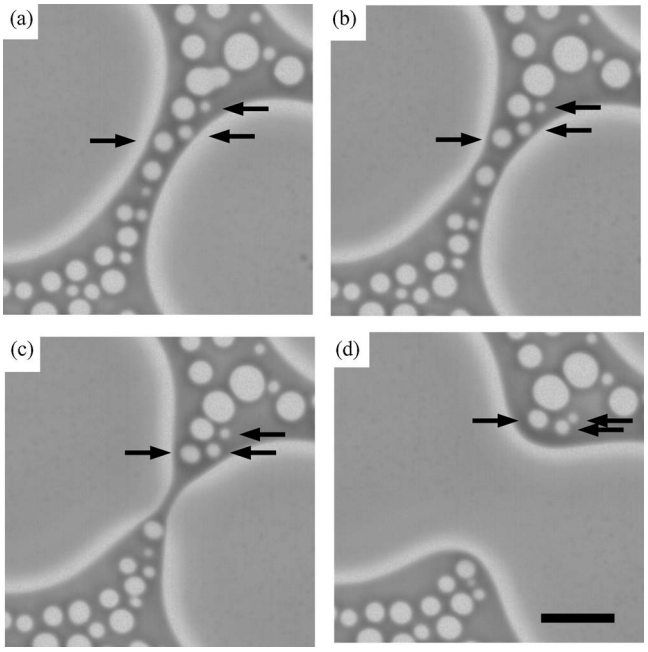

FIG. 7. A break of a micelle-rich domain, containing a number of water-rich bubbles, pulled by the surface tension. The motion of the bubbles shows the existence of a flow. The time of observation from the onset of the separation was: 14 s (a); 15 s (b); 16 s (c); 17 s (d). Arrows indicate the same bubbles moving in the time sequence. The scale bar is 0.25 mm.

Since the rims consist of the micelle-rich phase, there is no reason for them to diffuse away into the mother phase during the phase separation process. Thus, there is a transient three phase coexistence among the water-rich phase, the micelle-rich phase, and the mother phase, where the micelle-rich phase is always in between the water-rich phase and the mother phase. We believe that this is the first report investigating the concentration profile in the initial stage of the viscoelastic phase separation. We suggests that this type of a transient coexistence between metastable phases is a common feature of the viscoelastic phase separation.

As the water-rich nuclei grow, so do the rims. When they consume all the mother phase, the coarsening stage begins. Now rims become a network as shown in Fig. 2(b). The coarsening of the networks proceeds as their occasional breaks and shrinkage [Figs. 2(c)–2(e)]. In this stage, flows of the micelle-rich domains are obvious as shown in Fig. 7. Bubbles in a micelle-rich domain move according to its deformation, which indicates the existence of local flow in the domain. Thus the hydrodynamic flow dominates the coarsening process. It seems that other coarsening mechanisms, such as the Brownian coalescence or evaporation-condensation, do not operate here at least as a dominant mechanism.

The growth exponent, however, is not close to the unity or 2/3 as expected for a hydrodynamic coarsening,[3] as shown in Fig 5. The exponents obtained by the experiments are close to the value expected for the Brownian coalescence or the

evaporation-condensation mechanism. We will propose a simple model in Sec. IV B to explain the exponent observed in our system under the hydrodynamic coarsening.

Finally, micelle-rich domains form discs [Fig. 2(f)] as it is expected from the phase diagram (Fig. 1), which completes the phase inversion.

B. Breakdown of the scaling hypothesis and a coarsening model

The morphology characteristics, A, L, and χ shown in Fig. 4 can be used to test the dynamic scaling hypothesis, which assumes the existence of a single characteristic length scale and that a pattern is scaled by that length scale. It turns out as shown in Fig. 4(d) that the dynamic scaling does not hold at any moment of the phase separation process in our system. The breakdown of the scaling hypothesis was thought to be a common property of the viscoelastic phase separation.[28]

Taniguchi and Onuki reported that in their simulation for polymer solutions the viscoelasticity suppressed hydrodynamic flows and obtained a growth exponent about 1/3.[25] However, it was the hydrodynamic flow which dominates the coarsening in our system as discussed above. Let us estimate the Péclet number, which is the ratio of the rate of advection to the rate of diffusion,

$$Pe \equiv \frac{vl}{D} \simeq 10, \tag{2}$$

where the characteristic velocity $v \sim 10^{-6}$ m/s is estimated from the velocity of domains, the characteristic length $l \sim 10^{-4}$ m is obtained from Fig. 2, and the diffusion coefficient $D \sim 10^{-11}$ m^2/s used is the value of micelles in dilute solutions.[41] $Pe \sim 10$ signifies the importance of flow in our system.

Wagner and Yeomans reported using lattice Boltzmann simulations[32] that the scaling hypothesis can break down when diffusive coarsening and hydrodynamic coarsening maintain a certain balance, where the hydrodynamic coarsening mode makes smaller domains more circular quickly, but leaves elongated domains as elongated because of their small curvature. This makes the distribution of the domains bimodal. This is actually seen in Figs. 2(c)–2(f), where small circular domains coexisted with elongated domains.

The growth exponent obtained ($\alpha \simeq 1/3$) with hydrodynamic flows may be understood as follows.[42,43] Let us consider an elongated domain as shown schematically in Fig. 8. Under the non-slip boundary condition in a quasi-two-dimensional geometry, the dominant term in $\nabla^2\vec{u}$ of the velocity field $\vec{u}$ in the Navier-Stokes equation is $\partial^2\vec{u}/\partial z^2$, thus $|\nabla^2\vec{u}| \sim u/d^2$ for an elongated domain with the width a confined in a gap $d(\ll a)$ as shown in Fig. 8. Then the Navier-Stokes equation with the incompressibility condition is simplified to Darcy's law of laminar flow,

$$\eta \frac{u}{d^2} = |\nabla p|, \tag{3}$$

where p is the pressure. After the dimensional analysis of Siggia,[44] ∇p is estimated as the Laplace pressure, $p \sim \sigma/a$ with the surface tension σ, divided by the distance a, $|\nabla p| \sim \sigma/a^2$. With $u \sim \dot{a}$, Eq. (3) becomes $a^2\dot{a} \sim d^2\sigma/\eta$, which gives $a \sim t^{1/3}$. The $t^{1/3}$ growth was actually observed in simulations where the velocity field was calculated according to Darcy's law.[45]

Similarly, we can begin with the free energy of domains along with the phenomenological time evolution equation. The free energy of a domain illustrated in Fig. 8 is given by

$$G \sim \sigma \left(a + \frac{s}{a}\right) d \simeq \frac{\sigma s d}{a}, \tag{4}$$

where s is the area of a domain contacting to glass plates and $s/a^2 \gg 1$. Then the phenomenological time evolution equation

$$\dot{a} = -\Gamma \frac{\delta G}{\delta a} \tag{5}$$

leads to $a^2\dot{a} \sim \Gamma$, where Γ is the transport coefficient. If the dissipation for domain growth is proportional to s, and assuming that s is constant, $\Gamma \sim s^{-1}$ is also constant. Then we again expect $a \sim t^{1/3}$.

In order to check the validity of the model, we plot in Fig. 9 the interface density L_i of four different branches observed in Fig. 2. They were fitted by the function, $L_i(t) \sim (t - t_0)^{-\alpha}$, where t_0 is the time of break, to estimate α for each branch. The obtained value was $\alpha = 0.30 \pm 0.04$. This suggests that the entire coarsening obeys the power law growth with $\alpha \simeq 1/3$ because each branch obeys the same growth law, and that the domains do not interact with each other in the coarsening process. This agrees with the observation that majority of interface belongs to elongated domains, not to circular ones, and that the wetting layers do not induce attraction between these domains as mentioned in Sec. III.

The model tested above suggests, in short, that the coarsening process obeys incompressible fluid hydrodynamics and thus viscoelasticity relaxes completely in this stage. Since the

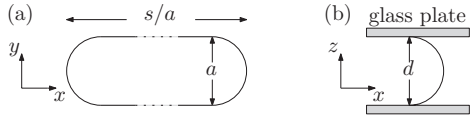

FIG. 8. A schematic representation of an elongated domain with the width a and the area s, confined in a gap $d(\ll a)$ between two glass plates. (a) a top view and (b) a side view.

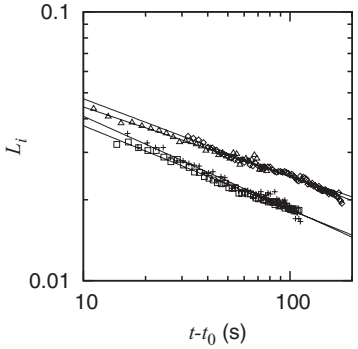

FIG. 9. Change of the interface density of a branch, L_i, for four chosen branches observed in the sample shown in Fig. 2. Each branch was disconnected at the one end at $t = t_0$, and was being absorbed into the network. The growth exponent, estimated by $L_i \sim (t - t_0)^{-\alpha}$, was 0.30 ± 0.04 where the error is the standard deviation.

coarsening starts about 10 s after the onset of the phase separation (Fig. 4), the time scale of the viscoelastic relaxation should be smaller than this time scale.

Let us finally discuss the role of the viscoelasticity in the pattern formation briefly. If there is no viscoelastic effect, the minority phase should nucleate and the pattern becomes circular. The hydrodynamic coarsening mode does not operate in circular patterns since there is no gradient of the Laplace pressure in the domains. Thus, we argue that the role of the viscoelasticity is to create elongated domains via the nucleation process of the majority phase. After the viscoelasticity relaxes completely, the coarsening is induced by flows, which produces the $t^{1/3}$ growth of domains under the non-slip boundary condition of quasi-two-dimensional ($d \ll a$) geometry.

V. CONCLUSIONS

We found that dilute surfactant $C_{12}E_5$ solutions exhibited the viscoelastic phase separation, where characteristic phenomena, such as the network pattern formation, the phase inversion, and the volume shrinking of domains, were observed. It was also found that the phase separation proceeded from the nucleation of the majority phase (water-rich phase), where nucleated domains were characteristically rimmed by the minority phase (micelle-rich phase). This created temporary three phase coexistence among the water-rich phase, micelle-rich phase, and the mother phase where the micelle-rich phase always existed between the water-rich phase and the mother phase. The viscoelasticity affected the pattern evolution significantly by creating elongated domains via the nucleation of the majority phase. The coarsening process was found to be dominated by hydrodynamic flows and did not obey the dynamic scaling hypothesis. The growth exponent obtained ($\alpha \sim 1/3$) was explained by a simple fluid model with Darcy's law of laminar flow, which suggested that the viscoelasticity relaxed completely in the coarsening stage.

ACKNOWLEDGMENTS

This work was supported by KAKENHI (Grant-in-Aid for Scientific Research) on Priority Area "Soft Matter Physics" from the Ministry of Education, Culture, Sports, Science, and Technology of Japan.

[1] J. D. Gunton, M. San Miguel, and P. S. Sahni, in *Phase Transitions and Critical Phenomena*, edited by C. Domb and J. L. Lebowitz (Academic, London, 1983), Vol. 8.
[2] K. Kawasaki and T. Ohta, Physica A **118**, 175 (1983).
[3] H. Furukawa, Adv. Phys. **34**, 703 (1985).
[4] A. J. Bray, Adv. Phys. **43**, 357 (1994).
[5] A. Onuki, *Phase Transition Dynamics* (Cambridge University Press, Cambridge, England, 2002).
[6] Y. C. Chou and W. I. Goldburg, Phys. Rev. A **20**, 2105 (1979).
[7] S. Nojima, Y. Ohyama, M. Yamaguchi, and T. Nose, Polymer J. **14**, 907 (1982).
[8] S. Nojima, K. Shiroshita, and T. Nose, Polymer J. **14**, 289 (1982).
[9] T. Hashimoto, M. Itakura, and H. Hasegawa, J. Chem. Phys. **85**, 6118 (1986).
[10] T. Hashimoto, M. Itakura, and N. Shimidzu, J. Chem. Phys. **85**, 6773 (1986).
[11] T. Kyu and J. M. Saldanha, Macromolecules **21**, 1021 (1988).
[12] C. Kedrowski and F. S. Bates, Macromolecules **26**, 3448 (1993).
[13] H. Takeno and T. Hashimoto, J. Chem. Phys. **107**, 1634 (1997).
[14] C. K. Haas and J. M. Torkelson, Phys. Rev. E **55**, 3191 (1997).
[15] H. Wang, R. J. Composto, E. K. Hobbie, and C. C. Han, Langmuir **17**, 2857 (2001).
[16] J. Hobley, S. Kajimoto, A. Takamizawa, and H. Furukawa, Phys. Rev. E **73**, 011502 (2006).
[17] R. Paul, U. Karabiyik, M. C. Swift, and A. R. Esker, Langmuir **24**, 5079 (2008).
[18] H. Tanaka, J. Phys.: Condens. Matter **12**, R207 (2000).
[19] J. H. Aubert, Macromolecules **23**, 1446 (1990).
[20] H. Tanaka, Phys. Rev. E **47**, 2946 (1993).
[21] S.-W. Song and J. M. Torkelson, Macromolecules **27**, 6389 (1994).
[22] H. Tanaka, Phys. Rev. Lett. **76**, 787 (1996).
[23] H. Tanaka, Y. Nishikawa, and T. Koyama, J. Phys.: Condens. Matter **17**, L143 (2005).
[24] H. Tanaka and Y. Nishikawa, Phys. Rev. Lett. **95**, 078103 (2005).
[25] T. Taniguchi and A. Onuki, Phys. Rev. Lett. **77**, 4910 (1996).
[26] R. Ahluwalia, Phys. Rev. E **59**, 263 (1999).
[27] H. Tanaka and T. Araki, Phys. Rev. Lett. **78**, 4966 (1997).
[28] T. Araki and H. Tanaka, Macromolecules **34**, 1953 (2001).
[29] J. Zhang, Z. Zhang, H. Zhang, and Y. Yang, Phys. Rev. E **64**, 051510 (2001).
[30] K. Luo, W. Gronski, and C. Friedrich, Eur. Phys. J. E **15**, 177 (2004).
[31] H. Tanaka and T. Araki, Chem. Eng. Sci. **61**, 2108 (2006).
[32] A. J. Wagner and J. M. Yeomans, Phys. Rev. Lett. **80**, 1429 (1998).
[33] T. Kalwarczyk, N. Ziebacz, S. A. Wieczorek, and R. Holyst, J. Phys. Chem. B **111**, 11907 (2007).
[34] R. Strey, R. Schomacker, D. Roux, F. Nallet, and U. J. Olsson, J. Chem. Soc. Faraday Trans. **86**, 2253 (1990).
[35] V. Sofonea and K. R. Mecke, Eur. Phys. J. B **8**, 99 (1999).
[36] K. R. Mecke, Phys. Rev. E **53**, 4794 (1996).
[37] H. Tanaka, Phys. Rev. Lett. **72**, 3690 (1994).
[38] H. Tanaka, J. Phys.: Condens. Matter **13**, 4637 (2001).
[39] A. Bernheim-Groswasser, E. Wachtel, and Y. Talmon, Langmuir **16**, 4131 (2000).
[40] T. Araki and H. Tanaka, Phys. Rev. E **72**, 041509 (2005).
[41] M. Lesemann, A. Martin, L. Belkoura, G. Fleischer, and D. Woermann, Langmuir **13**, 5289 (1997).
[42] A. J. Bray, Adv. Phys. **51**, 481 (2002).
[43] H. Tanaka, Europhys. Lett. **24**, 665 (1993).
[44] E. D. Siggia, Phys. Rev. A **20**, 595 (1979).
[45] A. Shinozaki and Y. Oono, Phys. Rev. A **45**, R2161 (1992).